NeuroImage 179 (2018) 225–234

Contents lists available at ScienceDirect

NeuroImage

journal homepage: www.elsevier.com/locate/neuroimage

GridLoc: An automatic and unsupervised localization method for high-density ECoG grids

Mariana P. Branco [1], Michael Leibbrand [1], Mariska J. Vansteensel, Zachary V. Freudenburg, Nick F. Ramsey [*]

Brain Center Rudolf Magnus, Department of Neurology and Neurosurgery, University Medical Center Utrecht, Utrecht, The Netherlands

ARTICLE INFO

Keywords:
Electrocorticography
High-density
Electrode localization
Unsupervised
Angiogram
Cortical distance
Resting-state
High-frequency band

ABSTRACT

Precise localization of electrodes is essential in the field of high-density (HD) electrocorticography (ECoG) brain signal analysis in order to accurately interpret the recorded activity in relation to functional anatomy. Current localization methods for subchronically implanted HD electrode grids involve post-operative imaging. However, for situations where post-operative imaging is not available, such as during acute measurements in awake surgery, electrode localization is complicated. Intra-operative photographs may be informative, but not for electrode grids positioned partially or fully under the skull. Here we present an automatic and unsupervised method to localize HD electrode grids that does not require post-operative imaging. The localization method, named GridLoc, is based on the hypothesis that the anatomical and vascular brain structures under the ECoG electrodes have an effect on the amplitude of the recorded ECoG signal. More specifically, we hypothesize that the spatial match between resting-state high-frequency band power (45–120 Hz) patterns over the grid and the anatomical features of the brain under the electrodes, such as the presence of sulci and larger blood vessels, can be used for adequate HD grid localization. We validate this hypothesis and compare the GridLoc results with electrode locations determined with post-operative imaging and/or photographs in 8 patients implanted with HD-ECoG grids. Locations agreed with an average difference of 1.94 ± 0.11 mm, which is comparable to differences reported earlier between post-operative imaging and photograph methods. The results suggest that resting-state high-frequency band activity can be used for accurate localization of HD grid electrodes on a pre-operative MRI scan and that GridLoc provides a convenient alternative to methods that rely on post-operative imaging or intra-operative photographs.

Introduction

Subchronic and acute electrocorticography (ECoG) are increasingly used in the clinical and scientific communities in order to investigate and map brain-functions and understand brain-disorders (Jacobs and Kahana, 2010). ECoG is a technique that acquires brain signals via electrode grids or strips that are placed directly on the cortical surface (Freeman et al., 2000; Crone et al., 1998; Lesser et al., 2010), without penetrating the cortical tissue. Typical clinical grids used to localize seizure foci in patients with intractable epilepsy have an inter-electrode spacing of 1 cm (Salles et al., 1994; Diehl and Lüders, 2000; Lesser et al., 2010). These grids have also been used in other applications, ranging from neurostimulation of the cortex of epilepsy patients to reduce seizure occurrence (Heck et al., 2014), to providing stroke patients with neurofeedback for rehabilitation (Gomez-Rodriguez et al., 2011) and Brain-Computer Interfaces (Leuthardt et al., 2004; Vansteensel et al., 2016). In recent years, however, electrode grids with higher spatial resolution have been increasingly used to facilitate the diagnosis of neural pathophysiology (Van Gompel et al., 2008) and for brain research (Slutzky et al., 2010; Flinker et al., 2011; Siero et al., 2013; Bouchard and Chang, 2014; Branco et al., 2017a). Indeed, ECoG grids with increased spatial density, hereafter referred to as high-density (HD) grids, are particularly useful for investigating fine-scale cortical dynamics (Kellis et al., 2016; Wang et al., 2016), given the fact that electrodes spaced as close as a few millimeters still provide discriminable information (Slutzky et al., 2010; Siero et al., 2013).

* Corresponding author. Brain Center Rudolf Magnus, Department of Neurology and Neurosurgery, University Medical Center Utrecht, P.O. Box 85500, 3508 GA, Utrecht, The Netherlands.

E-mail address: N.F.Ramsey@umcutrecht.nl (N.F. Ramsey).

[1] These authors contributed equally to this work.

https://doi.org/10.1016/j.neuroimage.2018.06.050
Received 28 February 2018; Received in revised form 25 May 2018; Accepted 15 June 2018
Available online 18 June 2018

Table 1
Patient and HD-ECoG grid information.

Subject No.	Age at implantation	Gender	Implanted hemisphere	Type of recording	No. Included electrodes	Interelectrode distance (mm)	Exposed diameter (mm)	Grid dimensions (# electrodes)	HD grid Manufacturer	Imaging scans	CT scan resolution (mm)
S1	18	Male	Left	Chronic	60	3	1.3	8 × 8	AdTech[1]	CT, T1,MRA	0.43 × 0.43 ×0.5
S2	19	Male	Left	Chronic	32	3	1.3	8 × 4	AdTech1	CT, T1,MRA	0.5 × 0.5 ×0.7
S3	19	Female	Left	Chronic	32	3	1.3	8 × 4	AdTech[1]	CT, T1	0.6 × 0.6 ×0.6
S4	28	Male	Right	Acute	62	3	1.3	8 × 8	AdTech[1]	MRI	–
S5	19	Male	Left	Chronic	59	4	1	8 × 8	PMT Corporation[2]	CT, T1	0.5 × 0.5 x 1
S6	22	Male	Left	Chronic	63	4	1	8 × 8	PMT Corporation[2]	CT	0.5 × 0.5 × 0.7
S7	53	Female	Left	Acute	63	3	1	16 × 8	PMT Corporation[2]	T1	
S8	39	Male	Left	Acute	124	3	1	16 × 8	PMT Corporation[2]	T1	

CT- Computed tomography; T1 – T1 weighted structural scan; MRA – Magnetic Resonance Angiogram; T1+gd – T1-weighted structural scan with gadolinium contrast; [1]Racine, WI, USA; [2]Chanassen, MN, USA.

In both clinical and research applications of HD-ECoG, the precise localization of each contact point is crucial to accurately pinpoint the source of activity. To date, the available HD-ECoG localization methods make use of post-operative Computed Tomography (CT) scans (Branco et al., 2017b; Hamilton et al., 2017). In the absence of post-operative imaging, however, such as during intra-operative (awake) recordings, or when post-operative imaging provides insufficient or no information about the implanted electrodes, there is currently, to our knowledge, no technique available that allows for accurate localization of HD-ECoG grids. For intra-operative cases (e.g., Jiang et al., 2015), HD grids could potentially be localized using intra-operative localization methods currently used to localize standard clinical grids and which make use of a neuronavigator (Gupta et al., 2014), intra-operative photography, or intra-operative fluoroscopy (Randazzo et al., 2016). However, these methods have not been validated for HD grids and are not suitable for electrodes hidden from view (under the skull).

Here we present a novel method for HD grid localization on the basis of ECoG resting-state signals combined with pre-operative MRI information of the brain structure and vasculature. This method is based on two hypotheses. First, based on a previous study that showed that larger blood vessels attenuate the high-frequency band (HFB) power recorded from clinical ECoG electrodes (Bleichner et al., 2011), we postulate that this effect would also be present in HFB ECoG recordings of HD grids. Second, since the distance between the electrode and the cortical surface is likely to influence the acquired signal amplitude, we further postulate that HFB power is also attenuated in electrodes over a sulcus.

We tested the above hypotheses by comparing the HFB pattern, as estimated based on the postulated attenuation effects at the grid localization computed using post-operative CT images (Hermes et al., 2010), with the actual measured HFB pattern. For this, data was used from 5 subjects for whom a CT-scan was available. Since the standard localization methods can only estimate but not determine true electrode locations relative to the cortex (due to brain shift and assumptions about projecting electrodes to the cortical surface in the pre-operative MRI), we then evaluated whether we could determine grid location solely based on the attenuation effects. For this we developed and tested a method, named GridLoc (Grid Localization), for finding the best fit between estimated and measured HFB patterns by allowing the grid to shift and rotate. This method was evaluated in 8 patients scheduled for or undergoing epilepsy surgery. Since there is no ground truth reference to compare results with, we report the gain in agreement between measured and estimated HFB values as compared to CT-based localization, and display the optimal position relative to the position obtained with the accepted gold-standard methods, such as a post-operative imaging or intra-operative photos (Hermes et al., 2010; Branco et al., 2017b).

Materials and methods

Subjects

Data from 8 patients who underwent surgery for removal of their focus of epilepsy were used. Six subjects (S1-S6) were implanted with ECoG grids 5–7 days before resection (chronic grids) and two only underwent ECoG during surgery (acute grids). All patients were implanted with high-density (HD) ECoG grids (Table 1) and gave consent to participate in the study. For 5 subjects (S1-3 and S5-6), the electrode positions, as predicted with the new GridLoc method (detailed below), were compared with locations obtained with a standard localization method (Hermes et al., 2010; Branco et al., 2017b), where the clinical post-operative CT scan (Philips Tomoscan SR7000, Table 1) was co-registered with their structural MRI scan. For the other three subjects (S4, chronic grid; and S7 and S8, acute grids) the GridLoc electrode positions were compared with (visible) locations determined with intra-operative photographs (Hermes et al., 2010). The study was approved by the ethical committee of the University Medical Center Utrecht, in accordance with the Declaration of Helsinki (2013).

ECoG data acquisition and analysis

Resting-state HD-ECoG data was recorded for 3 min from 7 subjects (S1-S6 and S8), and for 1.5 min from S7. Two systems were used for recording, being a 128-channel Micromed recording system (Treviso, Italy; hardware band-pass filter 0.15–134.4 Hz; sampled at 512 Hz), and a BlackRock system (Salt Lake City, USA; sampled at 2000 Hz). After confirming that data did not contain epileptic events nor burst suppression (as determined by a qualified clinician), the data were analyzed offline using the *Fieldtrip Toolbox* (Oostenveld et al., 2011) in a MATLAB® environment. All signals were first band-pass filtered (0.5–134 Hz) and notch filtered at 50 and 100 Hz to remove line noise. Subsequently, the signals were re-referenced using the common average reference (CAR) of all included HD-ECoG channels. Some channels were excluded because of broken leads, flat or abnormally noisy signals (Table 1). Frequency analysis was performed using the Morlet wavelet dictionary, with multiplication in the frequency domain (length equal to 3 standard deviations of the implicit Gaussian kernel and width 7 cycles). High-frequency band (HFB) power was extracted for the frequency range of 45–120 Hz in steps of 1 Hz (or 2 Hz in case of 2000 Hz sampling frequency), and averaged across all bins. The HFB power signals were extracted per channel and averaged over time. The measured distribution of HFB power over the grid was taken as the *measured HFB pattern*.

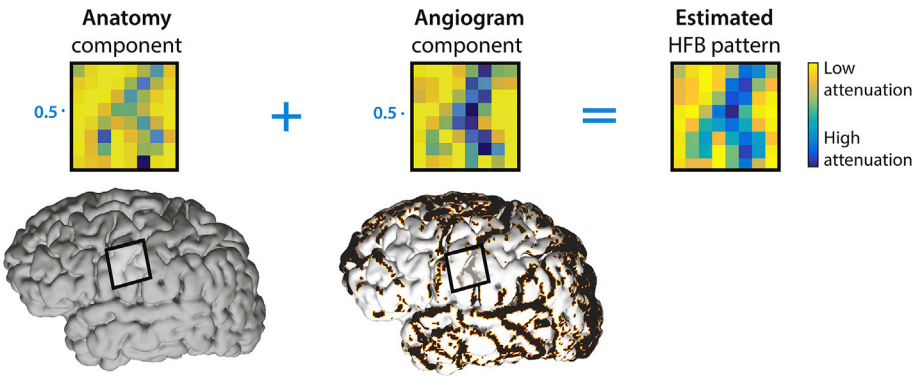

Fig. 1. Computation of the estimated HFB pattern. Example of the computation of the estimated HFB pattern computed for subject S1 at the specific grid location indicated by the black square. For each electrode on the 8 × 8 grid (matrix) the estimated HFB values were computed by summing the anatomy and angiogram components with equal weights (0.5). Each component is represented as values between dark blue (i.e., lower signal amplitude, high attenuation) and yellow (i.e., higher signal amplitude, low attenuation). The anatomy component was computed by measuring the distance between the electrodes and the cortical surface. The angiogram component (black vessels on the brain cortical surface) was based on the number of vertices identified as a vessel within 3 mm from the electrode.

Anatomical and vascular acquisition analysis

For each subject, a 3T structural MRI scan (T1-weighted) was acquired (Philips Achieva, Best, The Netherlands). For two subjects (S1 and S2), Magnetic Resonance Angiogram (MRA) scans were also acquired at 3T to localize the blood vessels using a 3D gradient echo sequence (phase contrast angiography, Philips Achieva, Best, The Netherlands). The resolution of both types of scans was 1 mm isotropic (whole brain). For two other subjects (S7 and S8) a structural MRI was performed with gadolinium contrast, which provided vascular contrast (albeit less detailed than an MRA). For S7 this scan was of poor quality, but it provided suitable information for the central part of the HD grid (64 of the 128 electrodes, see Table 1). For each subject, the cortical surface model was obtained by segmentation of the structural MRI, using FreeSurfer (https://surfer.nmr.mgh.harvard.edu/). This generates a triangular mesh lining the surface (including sulci), in which every vertex represents a point in an [X,Y,Z]-coordinate space with a specific value (weight).

To test our hypotheses, we defined a model that estimates the HFB attenuation pattern (i.e., the *estimated HFB pattern*) based on vascular and cortical features, hereafter defined as the angiogram component and the anatomy component:

$$\text{Estimated HFB Pattern} = \alpha \cdot \text{Angiogram} + \beta \cdot \text{Anatomy} \quad (1)$$

with α and β being the model component weights. For the model, an equal contribution from each component was assumed ($\alpha = \beta = 0.5$).

A degree of attenuation was assigned to each electrode in the grid (Fig. 1), based on these two components. The angiogram component contributes to the model with the attenuation that arises from the presence of blood vessels under the electrode, as identified by an MRA or structural MRI scan with gadolinium contrast. These scans were first co-registered to the individual T1-weighted scans in SPM12 (http://www.fil.ion.ucl.ac.uk/spm/). The angiogram intensity values were thresholded manually, such that the vessels were optimally displayed on the cortical surface mesh. Subsequently, the angiogram values were normalized (between 0 and 1) and displayed on the cortical surface model (using standard methods). Lastly, the normalized values were inverted such that 0 represented a vessel (smallest signal amplitude,

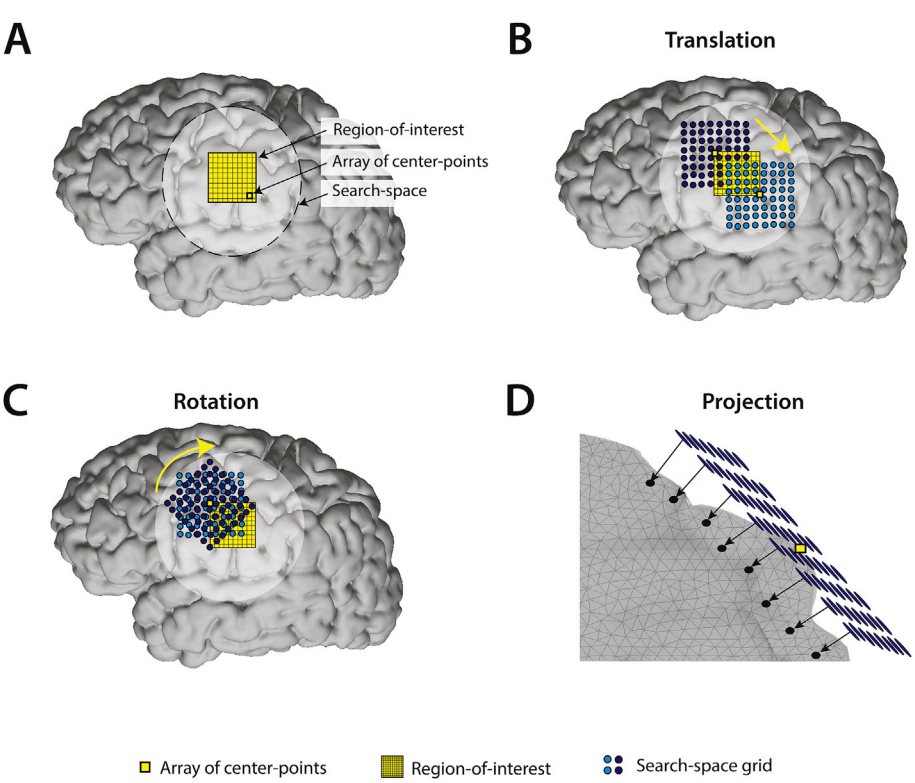

Fig. 2. Search-space. (A) A region-of-interest (ROI, yellow squared-grid) is defined as the complete set of N x N array of center-points (small yellow square), in which a grid template will be centered and which are spaced 1 mm apart. The search-space is the combined area of all possible grid template location (i.e., combinations of translations (B) and rotations (C)). (B) Each grid is translated through all points in the ROI and (C) rotated around its center from −45° to 45°. For each point in the array of center-points and rotation angle the grid template (see light and dark blue circles for two examples of grid positions) is projected from the tangent plane to the cortical surface (D).

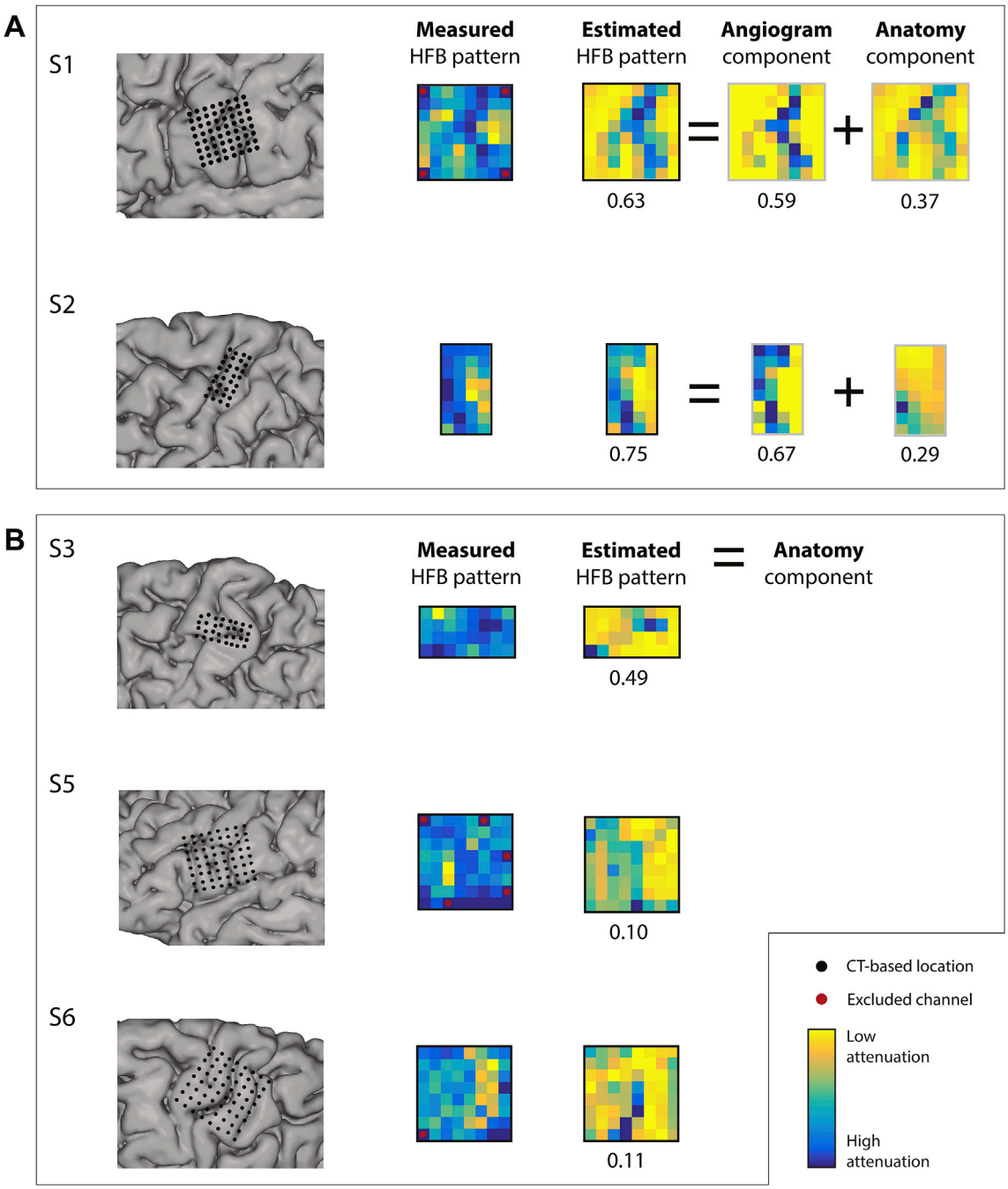

Fig. 3. Comparing measured and estimated HFB patterns at the CT-based grid location. (A) For two subjects, S1 and S2, both angiogram and anatomy components were available. The HFB pattern was compared with the estimated HFB pattern, the angiogram and the anatomy components by means of Pearson correlations (correlation values are indicated below). The estimated HFB pattern is the result of the equally-weighted sum of the angiogram and anatomy components. (B) For three subjects, S3, S5 and S6, the angiogram component was not available. (A–B) The grid location computed using post-surgical CT scans is shown on the left column (black dots). Electrodes excluded from analysis are marked with a red circle on the measured HFB patterns. The color-map represents low (dark blue) and high (yellow) attenuation levels.

higher attenuation) and 1 otherwise (largest signal amplitude, lower attenuation). All vertices with a value between 0 and 1 were set to 0 to increase the visibility of the blood vessels. Considering this factor, we calculated the average angiogram value of the vertices located within a 3 mm radius from each inspected electrode coordinate. This then resulted in a (mean) value between 0 and 1 per electrode, where a value close to 0 means there are blood vessels located in the direct vicinity ($\leq$3 mm radius) of the electrode coordinate and a value of 1 means that there are no blood vessels located in the direct vicinity of the electrode.

The anatomy component represents the Euclidean distance from the electrode location to the cortical surface model. For that, the mean normal vector of the vertices within 25 mm of an electrode coordinate was used to project the electrodes onto the cortical surface. Both the normal vector and the subject's cortical model were based on the freely available *NeuralAct Toolbox* (described by Algorithm 1 in Kubanek and Schalk, 2015). The Euclidean distances from the electrodes to their projections onto the surface model (along the averaged normal vector) were then also normalized between 0 and 1, such that 1 was the smallest distance to the surface (lower attenuation) and 0 the largest (higher attenuation).

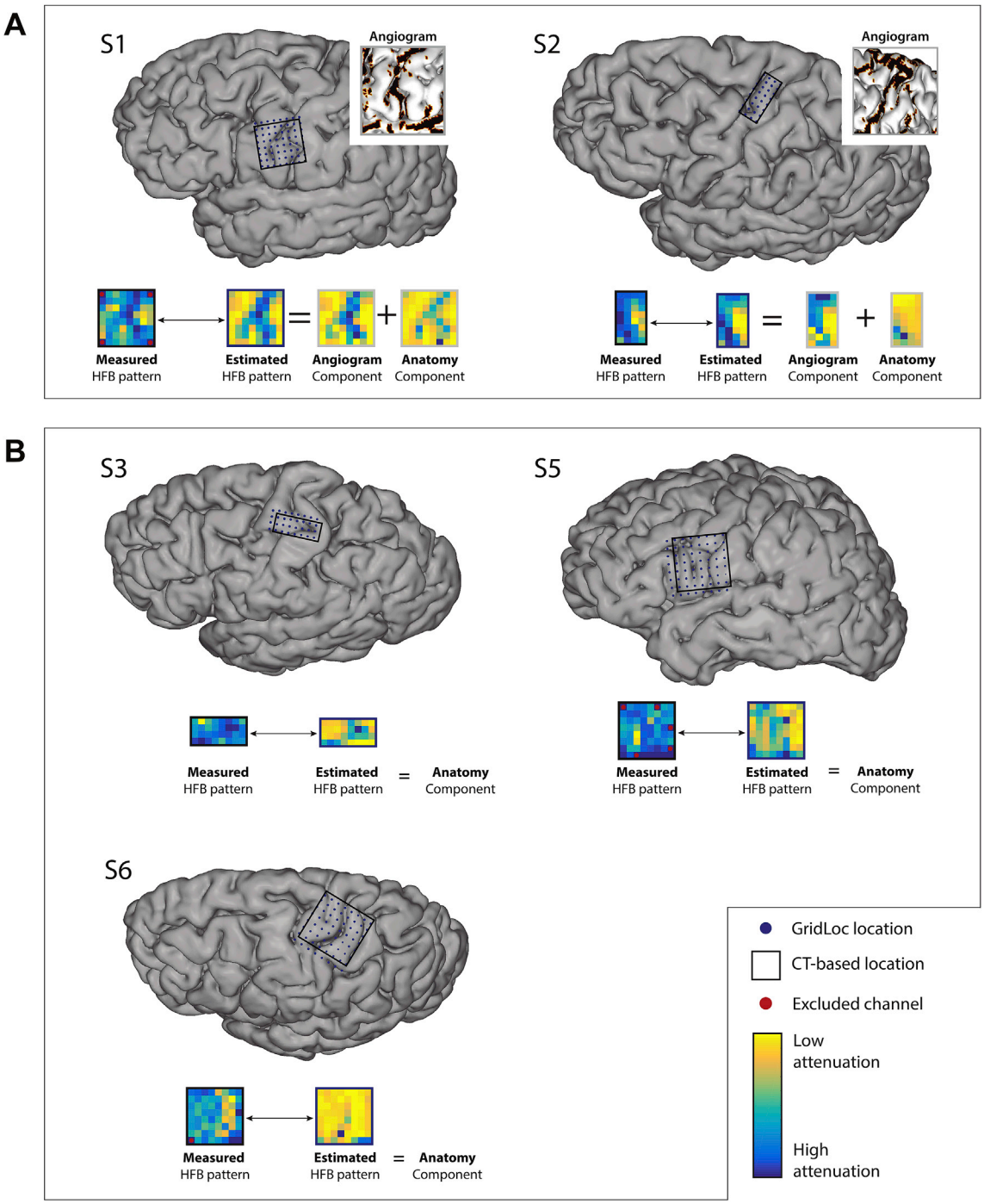

Fig. 4. Validation of the electrode grid position for five subjects using post-operative CT. (A) For two subjects both the angiogram and anatomy components and post-operative CT were available. The estimated grid position (blue circles) is displayed together with the CT-based grid position (black squares), as detected using the CT scan. The angiogram component is displayed for each subject for the region of interest (insert). The measured HFB spatial pattern was correlated with the estimated HFB pattern at every grid location, except for the excluded channels (marked with red dots). The highest correlation yielded the estimated grid position. (B) For three subjects the angiogram component was not available, hence the grid prediction was based solely on the anatomy component. All spatial patterns are displayed using a color-map where yellow represents low signal attenuation, and blue represents high signal attenuation.

Evaluation of the postulated attenuation patterns

In a first step, we assessed how well the above model predicts the measured HFB patterns. For that, the estimated HFB pattern was compared to the measured HFB pattern by means of a Pearson correlation. The estimated HFB pattern was computed for 5 subjects (S1-S3, S5 and S6) for whom a CT scan was available. In order to determine which model component (angiogram and anatomy) best estimated the HFB pattern, the correlation to each component separately was also computed. To assess the statistical significance of the correlation values, we randomly permuted the HFB values 1000 times in order to obtain an empirical null distribution of correlation values on random observation (Combrisson and Jerbi, 2015).

Table 2
Summary of the GridLoc results per subject.

Subject No.	Mean difference GridLoc and CT/photography (mm)	Standard deviation of difference (mm)	Correlation Measured and Estimated HFB pattern	Available components	Validation method
S1	1.31	0.47	0.70	Anatomy and angiogram	CT
S2	0.56	0.33	0.89	Anatomy and angiogram	CT
S3	2.64	0.34	0.64	Anatomy	CT
S4	1.35	0.64	0.61	Anatomy	Intra-operative photo
S5	2.71	0.45	0.50	Anatomy	CT
S6	3.14	0.52	0.39	Anatomy	CT
S7	1.44	0.86	0.46	Anatomy and angiogram	Intra-operative photo
S8	1.00	0.30	0.68	Anatomy and angiogram	Intra-operative photo
Mean	**1.94**	**0.51**	**0.62**		
SEM	**0.11**				

Evaluation of the GridLoc localization method

In a second step, we tested whether the use of the postulated model could be used to determine the position of HD grids on the brain. For that we developed an unsupervised and automatic method (GridLoc) that estimates the grid position. The GridLoc method iteratively moves the grid over the cortical surface area and computes the correlation between the measured HFB spatial pattern and the estimated HFB pattern computed with equation (1) at each step. The highest correlation indicates the best (estimated) grid position. The initial center and orientation of the grid is specified *à priori* by the user. From there, the search for the best fit is conducted unsupervised. The search-space is defined as follows: first, a region-of-interest (ROI) is defined by N x N array of center-points, spaced 1 mm apart (Fig. 2A). A two-dimensional grid template, with the same inter-electrode spacing as the implanted grid, is defined on the plane tangent to the cortex at the initial starting point and is translated within the ROI to every point (Fig. 2B). The grid template is additionally rotated up to a 45° angle with 1° increments in each direction, to account for different grid orientations within the ROI (Fig. 2C). The search-space is then defined as the combined area of all possible grid template positions. For every translation and rotation, the electrodes on the grid template are projected to the cortex (Fig. 2D) (Kubanek and Schalk, 2015). For each projected grid position the Pearson correlation was computed, and the position with the highest correlation was denoted the *estimated grid position*. Moreover, the estimated grid position was also computed using each model component (angiogram and anatomy) separately. To assess the significance, a non-parametric permutation test was used (Combrisson and Jerbi, 2015), where the correlation values for all grid positions were used to determine the empirical null distribution. Finally, for each subject the estimated grid position was compared with the one determined with the standard method described before (with post-operative CT or intra-operative photography), yielding a mean and standard deviation of distances between electrodes of both methods.

Results

Correlation between measured HFB and estimated HFB patterns

For all 5 subjects with an available CT scan, the correlation between the measured HFB and estimated HFB patterns was positive. For subjects S1 and S2 (Fig. 3A), for whom an angiogram was available, the measured HFB pattern significantly correlated with the estimated HFB pattern, with correlations values of 0.63 and 0.75 (p-value < 0.001), respectively. For these two subjects, the angiogram component seemed to correlate higher than the anatomy component (0.59 and 0.67, against 0.37 and 0.29, respectively), but not as high as the two components combined (Fig. 3A). For three other subjects (S3, S5 and S6, Fig. 3B), only the anatomy component was available. The correlations were 0.10, 0.11 and 0.49, for S5, S6 and S3 respectively, of which only the last was significant (p-value < 0.001). Overall, the results indicate that the model significantly predicts the measured HFB spatial patterns at the known grid position, and that the combination of both the angiogram and anatomy components can explain the HFB patterns better than any of these components alone.

Notably, in the model, the two components (angiogram and anatomy) were summed with equal weights (Equation (1), $\alpha = \beta = 0.5$). To investigate if these weights yielded optimal results, a weight optimization was carried out by comparing all possible combinations of $0 \leq \alpha \leq 1$ and $0 \leq \beta \leq 1$ (with the constraint $\alpha + \beta = 1$). Optimal settings per subject yielded a minor mean increase across subjects of the correlation values of only 0.04. Hence, all results shown here use equal weights.

GridLoc optimization results

The initial ROI center was specified per subject and the ROI size used was 11 mm × 11 mm for subjects S1-S6 and S8. For S7, an ROI of 18 mm × 18 mm was chosen because the grid center was hard to determine from the intra-operative photograph due to the angle of view. As a result, there were 121 or 324 center-points around which the grids were positioned (see section 2.7) and a total of 121 × 90° or 324 × 90° grid locations to test.

For five subjects (S1-S3 and S5-S6), the location as predicted using GridLoc was compared with the ones computed using a method based on post-operative CT scans (Fig. 4). For these subjects, the mean Euclidean difference between the two methods was 2.45 ± 0.16 mm (mean ± SEM, Table 2). The mismatch between the two positions was mainly caused by small translations and rotations. For three subjects (S4, S7 and S8), validation was carried out by comparing the estimated grid position (Fig. 5) to the operative photos (explantation photo for S4; and intra-operative photo for S7 and S8). For that, the 2D distance between the electrodes on the rendered brain and the operative photo was computed. This procedure, previously used in (Hermes et al., 2010), uses anatomical features, such as sulci and blood vessels to match the brain rendering to the intra-operative photograph (Supplementary Figures 1, 2 and 3). Results (Table 2) showed a mean (±std) distance between the GridLoc prediction and electrodes visible on the intra-operative photograph of 1.35 ± 0.64 mm for S4, 1.44 ± 0.86 mm for S7 and 1.00 ± 0.30 mm for S8. Overall, the estimated HFB patterns correlated well with the measured HFB pattern, yielding a mean correlation of 0.62 ± 0.15 (p-value < 0.001 for all subjects, Table 2). The model explained, thus, on average 38% of the resting-state HFB power variation across electrodes. This correlation was significantly higher than the correlation between the measured HFB pattern and the estimated HFB pattern obtained at the

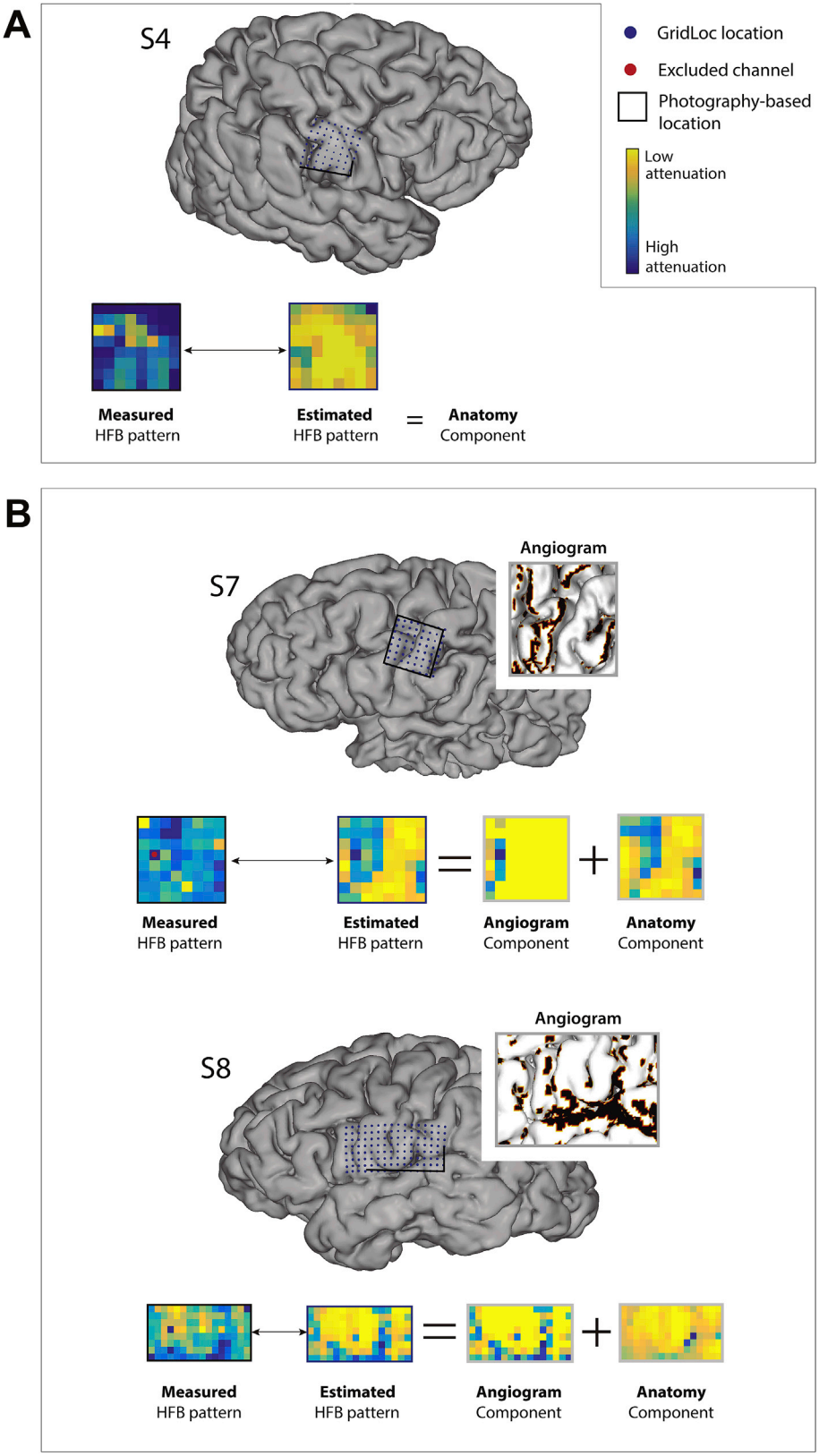

Fig. 5. Validation of the electrode grid position for three subjects using intra-operative photographs. (A) Estimated electrode grid position (blue circles) using the GridLoc method for subject S4. This subject had no angiogram scan. The measured HFB spatial pattern was correlated with the estimated HFB pattern at every grid location. The highest correlation yielded the estimated grid position. (B) A structural MRI scan with gadolinium contrast was available for subjects S7 and S8, hence the model was composed of angiogram and anatomy components. The angiogram component is displayed for each subject for the region of interest (insert). (A–B) The estimated grid position is displayed together with the partial grid position based on the visible parts of the grid on the intra-operative photographs (black squares/corners estimated from Supplementary Fig. 2 and 3). The measured HFB spatial pattern was correlated with the estimated HFB pattern at every grid location, except for the excluded channels (marked with red dots). All spatial patterns are displayed using a color-map where yellow represents low signal attenuation, and blue represents high signal attenuation.

grid location computed using the CT-based method (see previous section; Wilcoxon signed rank test, median 0.49 against 0.64, $N = 5$, p-value < 0.05).

In order to assess which model component (angiogram or anatomy) best estimated the grid position, the latter was also calculated using each component independently. Results for 4 subjects, for whom both angiogram and anatomy components were available, showed that a prediction based on one component alone may converge to an erroneous position, while using both components the prediction converges to the optimal position as determined using standard methods (Fig. 6). For S7 and S8

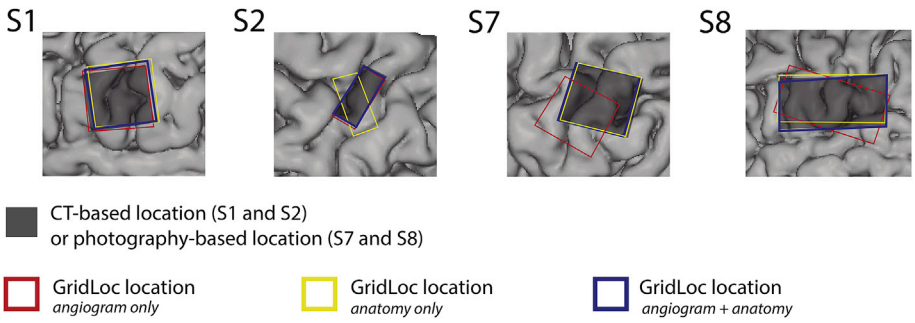

Fig. 6. GridLoc location using anatomy, angiogram or both components. GridLoc grid location predicted using a model based on the combined angiogram and anatomy components (blue square), angiogram alone (red square) or anatomy alone (yellow square) for four subjects (S1, S2, S7 and S8), for whom both angiogram and anatomy components were available. GridLoc positions are also compared with the CT-based (S1 and S2) or photography-based (S7 and S8; estimated from Supplementary Fig. 2 and 3) gold-standard location (black shaded square).

the CT-based location was not available, but the GridLoc position showed to be close to the grid position as derived from intra-operative photographs (see Table 2 and Supplementary Figures 2 and 3).

GridLoc computing time

The current method requires minimal user interaction, as it only requires the user to the set the center of the search-space and orientation of the grid and to define the angiogram threshold value. The algorithm subsequently performs an automatic and systematic search using a default precision (step-size) of 1 mm and 1°. These step-size values can be further decreased by the user, leading to higher precision at the expense of longer computational time. The time consumption of the GridLoc computation increases linearly with the size of the ROI and the number of electrodes.

Discussion

Evaluation of postulated attenuation patterns

Accurate localization of high-density intracranial grids is crucial for the valid interpretation of the acquired signals. Here, we hypothesized that the distance of an electrode to the cortical surface imposed by an underlying blood vessel and/or sulcus causes attenuation of the HFB power. HFB resting-state spatial power patterns were compared to a model where attenuation was introduced based on the presence of a blood vessel beneath the electrode and its distance to the cortical surface. The model was obtained from the grid position as estimated with a conventional CT-based method (Hermes et al., 2010; Branco et al., 2017b). The correlation between measured and estimated HFB patterns was highest when both angiogram and anatomy components were available. These results indicate that the amplitude of the HFB power is indeed attenuated in electrodes on sulci and large vessels, extending earlier results (Bleichner et al., 2011).

GridLoc grid localization

Based on the attenuation results, we then tested whether the use of such information could be used to determine the position of HD grids on the brain. The correlation between measured HFB pattern and estimated HFB pattern was optimized by means of iterative rotation and translation. For this, an automatic and unsupervised search algorithm was developed for finding the most likely grid position on the cortical surface using features from the ECoG data. The GridLoc method was applied to 8 subjects, four of whom had angiograms available. The resulting estimated grid positions were compared to those obtained with conventional methods using post-operative CT scans or intra-operative photos (Hermes et al., 2010; Branco et al., 2017b).

The estimated grid positions showed small rotation and translation displacements relative to the conventional location methods, with a mean difference of 1.94 mm (SEM = 0.11 mm) across all subjects. Additionally, the GridLoc method yielded a significant increase in correlation values (between measured HFB pattern and the estimated HFB pattern) as compared with correlation values based on the conventional CT-based location. Since there is no way to determine the true grid position, there is no objective way of assessing the accuracy of either the GridLoc or the conventional localization methods. However, taking above findings together, we argue that the GridLoc method may be more accurate than the conventional CT- or photograph-based approaches. It seems reasonable that this is due to the fact that the GridLoc method does not suffer from limitations inherent to the CT and intra-operative photos methods, in particular brain-shift-related electrode projection errors or inconsistent photograph angles, respectively.

Although the results showed a fair prediction using an anatomy component only, the best results were found for the subjects who also had an angiogram (S1, S2 and S8). That is, the model combining both components generally yielded the highest scores and the closest position to the positions obtained with the conventional methods. Hence, the GridLoc algorithm seems to work best when both anatomical and angiographic information are obtained before surgery.

Assumptions and limitations

The GridLoc method relies on three assumptions. Firstly, the current method relies on the structural and vascular geometry from which the grid is recording. That is, the method assumes that the inter-electrode distance is small enough and grid coverage is large enough to capture enough vessels and sulci to match a spatial pattern that is regionally unique. Hence, it may be expected that for HD-grids covering an area smaller than 1000 mm^2 (e.g., 32 electrodes, 3 mm inter-electrode distance), or with an inter-electrode distance larger than 4 mm, the specificity of the spatial pattern approaches a limit for an accurate localization.

Second, the method assumes that the inter-electrode distance is known and is constant, and that the distance between the tangent plane where the grid lays and the cortical surface is small enough, such that the inter-electrode distance between the electrodes is preserved after projection. This ignores the potential reduction of curvature of the cortical surface after deformation due to loss of ventricular cerebrospinal fluid (deflation typically results in surface shrinkage as the cortex flattens). With the projection of the 'deflated' cortex to the full pre-surgical cortical surface, electrode distances should ideally adapt to the increase in surface. This inaccuracy increases with total grid surface. One way to address this could be to allow inter-electrode distances to vary, to a certain degree, in the optimization procedure.

Third, the method also assumes that the HD grid position is roughly known and that only the exact position and orientation are yet to be determined. Indeed, the algorithm requires the setting of an initial

region-of-interest, which subsequently defines the search-space. This assumption is fair since grid positions are often carefully chosen by the surgeon. Uncertainty of the position can be addressed by increasing the search space which will affect computation time.

Several factors limit the quality of the data used. For one, angiograms did not always yield clear and complete blood vessel information. Since the results demonstrate that angiographic information is important for accurate localization, acquisition of high-quality angiogram images is warranted. The quality of the resting-state data, although difficult to determine, could have been also limited by inter-ictal activity or by anesthesia. However, such confounds are likely to produce a positive bias in our analysis, as they introduce a non-geometric suppression of the HFB, and would thereby limit the precision of the method. Hence, a degree of data inspection is advised for confound-free resting-state measurements.

Conclusion

We show that high-frequency band power is affected by factors that increase the distance between ECoG electrodes and the brain tissue. The power is attenuated in electrodes positioned on top of a blood vessel or on a sulcus. This phenomenon makes it possible to estimate the position of an electrode grid on the cortical surface based only on pre-operative structural and angiographic MR images, and a few minutes of resting-state ECoG data. Therefore, we present an automatic, unsupervised and accurate method for localization of high-density intracranial grids, named GridLoc, as an alternative to methods that rely on post-operative imaging or intra-operative photographs. The GridLoc software is customizable and allows the use of varying grid-, ROI- and step-sizes. The algorithm was developed in Matlab®, was tested in the Linux, Windows and Mac environments, and is freely available on github (https://github.com/UMCU-RIBS/GridLoc).

Acknowledgments

This research was funded by the ERC-Advanced 'iConnect' project (grant ERC-AdG 320708), the BrainGain Smart Mix Programme (grant SSM06011) and the Dutch Technology Foundation STW (grant UGT7685) (N.R.). The authors would like to thank Erik J. Aarnoutse, Frans S. S. Leijten, Cyrille H. Ferrier, Tineke Gebbink and the clinical neurophysiology team for the experimental environment and their help in collecting the data, Peter Gosselaar and Peter van Rijen for implantation of the grids, Efraïm Salari for helping to detect bad channels, Julia Berezutskaya for helping with the MRA projections and Dora Hermes for sharing the functions for projection of functional data onto the brain surface.

Appendix A. Supplementary data

Supplementary data related to this article can be found at https://doi.org/10.1016/j.neuroimage.2018.06.050.

References

Bleichner, M.G., Vansteensel, M.J., Huiskamp, G.M., Hermes, D., Aarnoutse, E.J., Ferrier, C.H., Ramsey, N.F., 2011. The effects of blood vessels on electrocorticography. J. Neural. Eng. 8 (4), 44002. https://doi.org/10.1088/1741-2560/8/4/044002.

Bouchard, K.E., Chang, E.F., 2014. Neural decoding of spoken vowels from human sensory-motor cortex with high-density electrocorticography. In: 2014 36th Annual International Conference of the IEEE Engineering in Medicine and Biology Society, August, pp. 6782–6785. https://doi.org/10.1109/EMBC.2014.6945185.

Branco, Mariana P., Freudenburg, Zachary V., Aarnoutse, Erik J., Bleichner, Martin G., Vansteensel, Mariska J., Ramsey, Nick F., 2017a. Decoding hand gestures from primary somatosensory cortex using high-density ECoG. Neuroimage 147 (February), 130–142. https://doi.org/10.1016/j.neuroimage.2016.12.004.

Branco, Mariana P., Gaglianese, Anna, Glen, Daniel, Dora Hermes, Saad, Ziad S., Petridou, Natalia, Ramsey, Nick F., 2017b. ALICE: a tool for automatic localization of intra-cranial electrodes for clinical and high-density grids. J. Neurosci. Meth. October. https://doi.org/10.1016/j.jneumeth.2017.10.022.

Combrisson, Etienne, Jerbi, Karim, 2015. Exceeding chance level by chance: the caveat of theoretical chance levels in brain signal classification and statistical assessment of decoding accuracy. Journal of Neuroscience Methods, Cutting-edge EEG Methods 250 (Suppl. C), 126–136. https://doi.org/10.1016/j.jneumeth.2015.01.010.

Crone, N.E., Miglioretti, D.L., Gordon, B., Lesser, R.P., 1998. Functional mapping of human sensorimotor cortex with electrocorticographic spectral analysis. II. Event-related synchronization in the gamma band. Brain 121 (12), 2301–2315. https://doi.org/10.1093/brain/121.12.2301.

Diehl, B., Lüders, H.O., 2000. Temporal lobe epilepsy: when are invasive recordings needed? Epilepsia 41, S61–S74. March. https://doi.org/10.1111/j.1528-1157.2000.tb01536.x.

Flinker, A., Chang, E.F., Barbaro, N.M., Berger, M.S., Knight, R.T., 2011. Sub-centimeter language organization in the human temporal lobe. In: Brain and Language, First Neurobiology of Language Conference: NLC 2009, vol. 117, pp. 103–109 (3). https://doi.org/10.1016/j.bandl.2010.09.009.

Freeman, Walter J., Rogers, Linda J., Holmes, Mark D., Silbergeld, Daniel L., 2000. Spatial spectral analysis of human electrocorticograms including the alpha and gamma bands. J. Neurosci. Meth. 95 (2), 111–121. https://doi.org/10.1016/S0165-0270(99)00160-0.

Gomez-Rodriguez, M., Grosse-Wentrup, M., Hill, J., Gharabaghi, A., Schölkopf, B., Peters, J., 2011. Towards Brain-Robot Interfaces in Stroke Rehabilitation.

Gupta, Disha, Jeremy Hill, N., Adamo, Matthew A., Ritaccio, Anthony, Schalk, Gerwin, 2014. Localizing ECoG electrodes on the cortical anatomy without post-implantation imaging. Neuroimage: Clinica 6, 64–76. https://doi.org/10.1016/j.nicl.2014.07.015.

Hamilton, Liberty S., Chang, David L., Lee, Morgan B., Chang, Edward F., 2017. Semi-automated anatomical labeling and inter-subject warping of high-density intracranial recording electrodes in electrocorticography. Front. Neuroinf. 11. https://doi.org/10.3389/fninf.2017.00062.

Heck, Christianne N., King-Stephens, David, Massey, Andrew D., Nair, Dileep R., Jobst, Barbara C., Barkley, Gregory L., Salanova, Vicenta, et al., 2014. Two-year seizure reduction in adults with medically intractable partial onset epilepsy treated with responsive neurostimulation: final results of the RNS system pivotal trial. Epilepsia 55 (3), 432–441. https://doi.org/10.1111/epi.12534.

Hermes, Dora, Miller, Kai J., Jan Noordmans, Herke, Vansteensel, Mariska J., Ramsey, Nick F., 2010. Automated electrocorticographic electrode localization on individually rendered brain surfaces. J. Neurosci. Meth. 185 (2), 293–298. https://doi.org/10.1016/j.jneumeth.2009.10.005.

Jacobs, Joshua, Kahana, Michael J., 2010. Direct brain recordings fuel advances in cognitive electrophysiology. Trends Cognit. Sci. 14 (4), 162–171. https://doi.org/10.1016/j.tics.2010.01.005.

Jiang, Tianxiao, Ince, Nuri, Jiang, Tao, Wang, Taylor, Mei, Shenshen, Li, Yunlin, Wang, Xiaofei, Sha, Zhiyi, 2015. Local spatial correlation analysis of hand flexion/extension using intraoperative high-density ECoG. https://doi.org/10.1109/EMBC.2015.7319806.

Kellis, Spencer, Sorensen, Larry, Darvas, Felix, Sayres, Conor, O'Neill III, Kevin, Brown, Richard B., House, Paul, Ojemann, Jeff, Greger, Bradley, 2016. Multi-scale analysis of neural activity in humans: implications for micro-scale electrocorticography. Clin. Neurophysiol. 127 (1), 591–601. https://doi.org/10.1016/j.clinph.2015.06.002.

Kubanek, Jan, Schalk, Gerwin, 2015. NeuralAct: a tool to visualize electrocortical (ECoG) activity on a three-dimensional model of the cortex. Neuroinformatics 13 (2), 167–174. https://doi.org/10.1007/s12021-014-9252-3.

Lesser, Ronald P., Crone, Nathan E., Webber, W.R.S., 2010. Subdural electrodes. Clin. Neurophysiol.: Offic. J. Int. Fed. Clin. Neurophysiol. 121 (9), 1376–1392. https://doi.org/10.1016/j.clinph.2010.04.037.

Leuthardt, Eric C., Schalk, Gerwin, Wolpaw, Jonathan R., Ojemann, Jeffrey G., Moran, Daniel W., 2004. A brain-computer interface using electrocorticographic signals in humans. J. Neural. Eng. 1 (2), 63–71. https://doi.org/10.1088/1741-2560/1/2/001.

Oostenveld, Robert, Fries, Pascal, Maris, Eric, Schoffelen, Jan-Mathijs, 2011. FieldTrip: open source software for advanced analysis of MEG, EEG, and invasive electrophysiological data. Intell. Neuroscience 2011 (January): 1 (1–1), 9. https://doi.org/10.1155/2011/156869.

Randazzo, Michael J., Kondylis, Efstathios D., Alhourani, Ahmad, Wozny, Thomas A., Lipski, Witold J., Crammond, Donald J., Mark Richardson, R., 2016. Three-dimensional localization of cortical electrodes in deep brain stimulation surgery from intraoperative fluoroscopy. Neuroimage 125 (January), 515–521. https://doi.org/10.1016/j.neuroimage.2015.10.076.

Salles, Antonio A. F. De, Swartz, Barbara E., Lee, Thomas T., Delgado-Escueta, Antonio V., 1994. Subdural recording and electrical stimulation for cortical mapping and induction of usual seizures. Stereotact. Funct. Neurosurg. 62 (1–4), 226–231. https://doi.org/10.1159/000098624.

Siero, Jeroen C.W., Hermes, Dora, Hoogduin, Hans, Luijten, Peter R., Petridou, Natalia, Ramsey, Nick F., 2013. BOLD consistently matches electrophysiology in human sensorimotor cortex at increasing movement rates: a combined 7T fMRI and ECoG study on neurovascular coupling. J. Cerebr. Blood Flow Metabol.: Offic. J. Int. Soc. Cerebr. Blood Flow and Metabol. 33 (9), 1448–1456. https://doi.org/10.1038/jcbfm.2013.97.

Slutzky, Marc W., Jordan, Luke R., Krieg, Todd, Chen, Ming, Mogul, David J., Miller, Lee E., 2010. Optimal spacing of surface electrode arrays for brain–machine interface

applications. J. Neural. Eng. 7 (2), 26004. https://doi.org/10.1088/1741-2560/7/2/026004.

Van Gompel, Jamie, J., Matthew Stead, S., Giannini, Caterina, Meyer, Fredric B., Richard Marsh, W., Fountain, Todd, So, Elson, Cohen-Gadol, Aaron, Lee, Kendall H., Worrell, Gregory A., 2008. Phase I trial: safety and feasibility of intracranial electroencephalography using hybrid subdural electrodes containing macro- and microelectrode arrays. Neurosurg. Focus 25 (3), E23. https://doi.org/10.3171/FOC/2008/25/9/E23.

Vansteensel, Mariska J., Pels, Elmar G.M., Bleichner, Martin G., Branco, Mariana P., Denison, Timothy, Freudenburg, Zachary V., Gosselaar, Peter, et al., 2016. Fully implanted brain–computer interface in a locked-in patient with ALS. N. Engl. J. Med. 375 (21), 2060–2066. https://doi.org/10.1056/NEJMoa1608085.

Wang, Po T., King, Christine E., McCrimmon, Colin M., Lin, Jack J., Sazgar, Mona, Hsu, Frank P.K., Shaw, Susan J., et al., 2016. Comparison of decoding resolution of standard and high-density electrocorticogram electrodes. J. Neural. Eng. 13 (2), 26016. https://doi.org/10.1088/1741-2560/13/2/026016.